Emittance preservation of an electron bunch in a loaded quasi-linear plasma wakefield

Veronica K. Berglyd Olsen* and Erik Adli
University of Oslo, Oslo, Norway

Patric Muggli
Max Planck Institute for Physics, Munich, Germany and
CERN, Geneva, Switzerland

(Dated: August 24, 2017)

We investigate beam loading and emittance preservation for a high-charge electron beam being accelerated in quasi-linear plasma wakefield driven by a short proton beam. The structure of the wakefield is similar to that of a long, modulated proton beam. By selecting transverse and longitudinal electron beam parameters in order to appropriately load the wake, we show that the bulk of the electron beam can be accelerated without significant emittance growth.

I. INTRODUCTION

Beam driven plasma wakefield accelerators have the potential to offer compact linear accelerators with high energy gradients, and has been of interest for several decades [1]. A relativist beam travelling through a plasma will excite a strong longitudinal e-field that can be loaded by a trailing witness beam. With optimal beam loading, the witness beam can have a high acceleration gradient. Acceleration of an electron beam by an electron drive bunch has been demonstrated experimentally [2–4] in the past. The AWAKE experiment at CERN is a proof of concept proton driven plasma wakefield accelerator [5].

A major challenge with plasma wakefield accelerators is, however, to produce an accelerated beam with a minimal increase in energy spread and emittance. In the well described linear case where the beam density n_b is much smaller than the plasma density n_0 the plasma causes emittance growth in the beam. A finite length beam will also see a varying transverse wakefield causing increasing energy spread [6]. In the non-linear regime, where $n_b > n_0$, the drive beam sees an unvarying transverse field due to a bubble forming in the plasma behind the drive beam. The bubble is formed by the transverse oscillations of the plasma electrons which move near uniformly as a function of distance from the drive beam, forming a sheet around an evacuated area. The much heavier plasma ions have no significant movement within the relevant time frame, and form an ion channel creating a focusing force that scales linearly with the radius. This produces an angularly symmetric focusing force [7, 8]. This effect also avoids the issue of increasing energy spread due to transverse beam loading. Increase in energy spread is still dependent on beam loading of the longitudinal e-field, E_z. Non-uniform beam loading can be negated by specially shaped beams that optimally flattens the field [6, 9], but this is difficult experimentally and is not a topic explored in this paper.

* v.k.b.olsen@cern.ch

A. Self-modulation as a Driver

A train of electron drive bunches with a separation λ_{pe} and a length $l_b \ll \lambda_{pe}$, where

$$\lambda_p = 2\pi \frac{c}{\omega_{pe}} \tag{1}$$

and

$$\omega_{pe} = \sqrt{\frac{n_0 e^2}{m_e \epsilon_0}}, \tag{2}$$

will drive an increasingly strong field E_z for each bunch [1]. A tailing witness beam loading the peak accelerating phase of this field will quickly gain energy from the wakefield. Acceleration of an electron witness beam driven by two electron drive beams was demonstrated at Brookhaven National Laboratory [10]. However, electron drive bunches will quickly lose energy to the plasma, and the accelerating witness beam will eventually catch up with the drive beam and the acceleration stop.

This de-phasing problem can be minimised by instead using a proton drive bunch [11]. Proton beams, like for instance the LHC and SPS beams at CERN, are ideal candidates for such an accelerator. However, they are orders of magnitude longer than the plasma wavelengths needed for such applications. This issue is resolved by letting the proton beam undergo self-modulation before injecting the witness beam into one of the buckets in the modulated structure. This self-modulation instability is caused by the transverse fields generated by the beam acting upon the beam itself, causing regions of the beam to rapidly defocus [12]. The modulation frequency is close to that of the plasma, and leaves a train of proton bunches along the beam axis with a surrounding halo.

B. The AWAKE Experiment

The AWAKE experiment, currently in its first stages of operation at CERN, uses the SPS beam as its driver. The first run of the experiment is set up with a 10 m rubidium vapour cell. The rubidium vapour is ionised by a

780 nm, 4.5 TW peak power laser with a pulse length of 100120 fs. The nominal plasma density of the AWAKE experiment is $7 \times 10^{14}\,\mathrm{cm}^{-3}$ [13]. This plasma density corresponds to a plasma wavelength $\lambda_{pe} = 1.26\,\mathrm{mm}$. The plasma density is matched to the SPS proton beam such that $k_{pe}\sigma_r = 1$ where $k_{pe} = 2\pi/\lambda_{pe}$ is the plasma wave number. The aim of the first phase of Run 1 of the experiment is to demonstrate self-modulation of the proton beam, and in 2018 to sample the wake field with a long electron bunch. The study presented here is for Run 2, which aims to demonstrate acceleration of a short electron bunch to high energy with a minimal increase in emittance and energy spread.

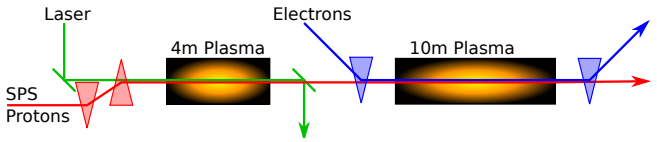

FIG. 1. A simplified illustration of the experimental setup for AWAKE Run 2. The SPS proton beam undergoes self-modulation in the first 4 m plasma cell. The electron witness beam is injected in one of the buckets, and undergoes acceleration in the second plasma cell [14, 15].

The preliminary design of the second run proposes to use two plasma sections, illustrated in figure 1. The first section of 4 m is the self-modulation stage where the proton beam undergoes self-modulation without the electron beam present. The electron witness beam will be injected into the modulated proton beam before stage two, where acceleration will occur. As the E_z-field will decrease due to the gap between the two cells, it is desirable to keep this as short as possible [15].

II. METHOD

The main focus of this study has been on the beam loading of the electron beam. In order to eliminate other factors that may affect this, we have tried several approaches to create a stable drive beam structure based on previous self- modulation studies.

Our first approach was to use a pre-modulated, short proton beam with similar structure to the one produced by the self-modulation of the SPS beam in AWAKE. These studies were done using the full PIC code Osiris [16] using 2D cylindrical-symmetric simulations. The proton beam was pre-modulated by a clipped cosine function to its longitudinal density profile, with a period matching λ_{pe}. Its transverse profile was kept as a Gaussian with $\sigma_r = k_{pe}^{-1} = 200\,\mu\mathrm{m}$. The length of the simulation beam was limited to $26 \cdot \lambda_{pe}$, and the electron beam injected after the 20th micro-bunch [14]. We performed several parameter scans with this setup, testing for the the maximum beam charge that could be accelerated with a high energy gain and low energy spread [15, 17].

In order to evaluate the quality of the beam, we also needed to study emittance evolution. However, full PIC codes like Osiris are vulnerable to numerical growth of emittance caused by the "numerical Cherenkov effect" [18]. This is a know issue with the Yee EMF solver which causes the phase velocity of electromagnetic fields to be lower than c while the beam moves very close to c. The effect can be mitigated somewhat by replacing the Yee solver with a solver designed by Lehe [19]. Our simulations showed that this numerical effect is still prominent in the high density regions of the electron beam, making it difficult to distinguish emittance growth from the physics from that originating from numerical error.

Quasi-static PIC codes do not suffer this problem, so in order to study the emittance evolution of the beam we instead turned to the recently released open source version QuickPIC developed by UCLA. QuickPIC is a fully relativistic 3D PIC code [20, 21].

A. Drive Beam Parameters

In the QuickPIC simulations we use a single proton drive bunch that sets up a wakefield comparable to that which we expect to see from the self-modulated SPS beam in AWAKE Run 2. The baseline AWAKE drive beam contains 3×10^{11} protons [13]. Only half of these are driving the wakefield, presuming the self-modulation is seeded in the middle of the unmodulated bunch. In addition. a significant portion of the protons are lost during self-modulation. The needed gap between the two plasma cells also contributes to a decreased density of protons near the axis, and some of the field is drained by other protons seeing an accelerating phase within the drive beam itself. In total, the expected peak E_z field of 2 GV/m in the first plasma cell drops to $500 - 600\,\mathrm{MV/m}$ in the second cell [22]. A single proton bunch of 1.46×10^{10}, or 2.34 nC and 7 kA was able to drive an E_z field of a comparable magnitude in our single drive bunch setup.

The single bunch approach also has the benefit of reducing simulation time for the 3D simulations. Our aim was to create a stable environment for the witness beam. We are not considering the evolution of the proton beam in this test setup, so to prevent the proton beam from evolving radially, we increased the drive beam particle mass by a factor of 1e^6.

The baseline AWAKE drive beam current is insufficient to reach the non-linear regime and produce a plasma bubble. The plasma electrons are depleted to around 65% of nominal plasma density at the injection point of the electron beam in reference simulations [22]. This condition is replicated in out single bunch case. The peak density of the drive beam is $0.83 \cdot n_0$ producing a quasi-linear condition behind it. The single bunch setup uses the baseline proton energy $W_{pb} = 400\,\mathrm{GeV}$, and retains the transverse size $\sigma_r = 200\,\mu\mathrm{m}$ throughout the plasma cell. The length of the drive bunch $\sigma_z = 40\,\mu\mathrm{m}$.

B. Witness Beam Parameters

The witness beam in our simulation differs from AWAKE baseline parameters on several key points. Initial beam energy is set such that $\gamma_{eb} = \gamma_{pb} = 426.3$. This was done to eliminate the problem of initial de-phasing of the witness beam. Beam loading of a short witness beam is sensitive to its position relative to the field [9]. AWAKE baseline energy for the long witness beam for Run 1 is $W_{eb} = 10 - 20\,\mathrm{MeV}$ [13]. In Run 2 the experiment will likely require a higher initial energy, but a $W_{eb} \approx 50\,\mathrm{MeV}$ is sufficient to minimise de-phasing as the drift $\Delta\xi \propto \gamma^{-2}$ [14]. For this case we have eliminated this source of de-phasing entirely in order to reduce the number of variables.

Earlier simulations with witness beam radius $\sigma_r = 100\,\mu\mathrm{m}$ caused the beam to undergo rapid transverse evolution as the beam entered the plasma region, reducing its σ_r from $100\,\mu\mathrm{m}$ to $< 10\,\mu\mathrm{m}$ [17]. This was primarily due to a mismatch between beam emittance and the plasma density. This relation is given by

$$\beta = \frac{\sigma_r^2}{\epsilon_g} = \frac{\lambda_p e}{2\pi}\sqrt{2\gamma_{rel}}, \tag{3}$$

where λ_p is the plasma wavelength.

In these simulations we have used a matched beam for an initial emittance of $2\,\mu\mathrm{m}$, corresponding to a σ_r of $5.25\,\mu\mathrm{m}$. The relatively small size of the witness beam compared to the proton beam put some restrictions on the transverse resolution of the witness beam. The transverse grid cell resolution was set to $1.17\,\mu\mathrm{m}$.

III. BEAM LOADING

The single drive beam setup is designed to behave similarly to the self-modulated case. However, since the drive beam is prevented from significant transverse evolution, we are presented with an idealised case where the electron witness beam sees consistent wakefields throughout the plasma stage. The E_z-field generated by the proton drive bunch is seen as the blue line in figure 2, shown with and without the electron beam present. With a proton beam density $n_{pb} \simeq n_0$, we are in the quasi-linear regime but near non-linear [23]. There is some depletion of plasma electrons, but not enough to form a bubble. The dashed green line in the lower part of figure 2 shows that the on-axis plasma density has a depletion of 67%, close to what we see in full scale reference simulations for AWAKE Run 2 [22].

The witness bunch generates its own wakefield, which in the accelerating phase partially cancels out the E_z field generated by the drive bunch. For a finite length bunch this causes the particles in the tail of the witness bunch to be accelerated less than those at the front resulting in higher energy spread in exchange for higher energy transfer [24]. Since $E_z \propto \rho_b$, a beam profile $\rho_b(\xi)$ that perfectly flattens the accelerating field within the witness beam will reduces energy spread to zero. The ideal shape is triangular or trapezoidal with the peak density in the direction of the beam velocity [6, 9].

For Gaussian beams a reasonable flat field, and consequently low energy spread, can be achieved by controlling the charge density to achieve a similar effect. This, however, puts the front of the witness bunch outside of the ideal region while the middle bulk of the beam has

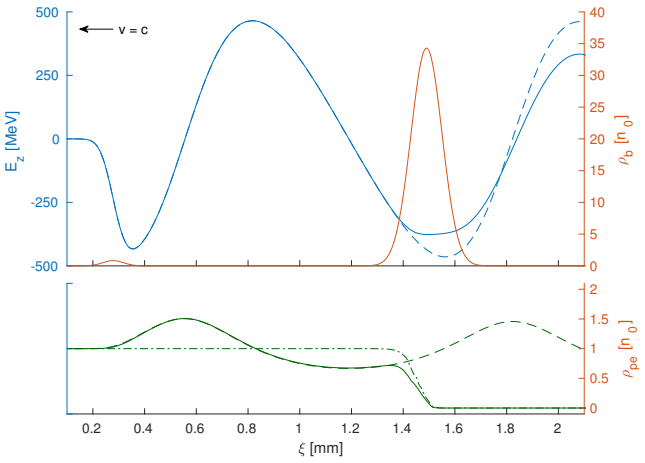

FIG. 2. The top plot compares the unloaded longitudinal e-field (no witness beam, blue. dashed line) and the loaded e-field (blue line) along the beam axis. The magnitude of the beam density along the axis is shown (red line) for reference. The bottom plot compares the plasma density along the beam axis for a drive beam with no witness beam (dashed green line), witness beam with no drive beam (dash-dotted green line), and both witness and drive beam present (continuous green line). $\xi = z - tc$ is the position in the simulation box and both beams travel towards the left. The beam and plasma densities arein units of initial plasma density $n_0 = 7 \times 10^{-14}\,\mathrm{cm}^{-3}$.

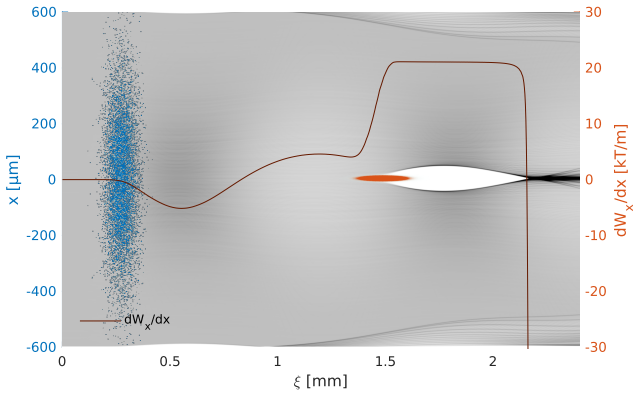

FIG. 3. The plasma density in grey with the proton beam (blue) and the electron beam (red) superimposed. The line plot indicates the transverse wakefield gradient dW_x/dx where $W_x = E_x - v_b B_y$, evaluated along the beam axis.

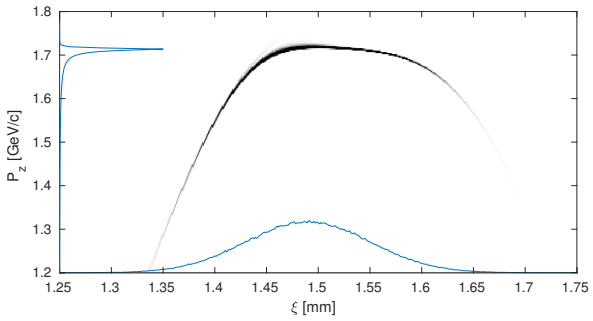

FIG. 4. Phase space charge distribution of a 100 pC, 60 μm long witness beam after 4 m of plasma. Mean momentum is 1.67 GeV/c with an RMS spread of 87 MeV/c (5.2%) for the full beam.

a trapezoidal-like shape. In our case, with a matched beam to the plasma density defined by equation 3, we are limited on how much total charge we can accelerate without reaching charge densities that will overload the field. The test case shown in figures 2 and 3 has a total charge of 100 pC with a $\sigma_r = 5.23\,\mu$m matching an initial normalised emittance $\epsilon_0 = 2\,\mu$m.

As illustrated in figure 4 our base case of a 100 pC, 60 μm long witness beam, as expected, shows a difference in energy transfer to the tail of the beam compared to the centre where the E_z-field is nearly flat. Also the front of the beam has a large tail in momentum space as this regions sees a consistently smaller accelerating field. The positioning of the witness beam is chosen to put the bulk of the charge as close to the peak accelerating field as possible.

Due to the high charge density resulting from a very narrow beam, the witness beam's own wakefield reaches the full non-linear regime with $n_{eb} \approx 35 \times n_0$. This second wakefield is driven by the beam's own front. The space charge rapidly becomes high enough to start expel plasma electrons from the beam axis, and form the characteristic electrons sheet that defines the blowout regime. As a result the plasma region reaches full depletion close to the peak of the electron beam, which in turn generates strong focusing fields, with gradients of 20 kT/m near the beam axis (see figure 3).

The witness beam's self-generated bubble prevents the tailing end of the beam to see any significant emittance growth. For the majority of the cases we studied that maintained a stable accelerating structure, about 70 − 80% of the beam retained its initial emittance. Figure 5 shows the 100 pC and $\sigma_z = 60\,\mu$m case extended to a 100 m plasma and the drive beam energy increased to 7 TeV (LHC energy) to prevent de-phasing. De-phasing for the SPS beam case starts to become significant after about 50 m.

The on-axis density of the electron beam increases as its gamma factor increases and its transverse size decreases. The beam radius follows the evolution given by equation 3 with $\lambda_{pe} = \lambda_0$ for the section of the beam where normalised emittance is preserved. This has the potential to cause overloading of the field. However, our 100 pC case is slightly under loaded, and this does not seem to be a significant effect in this instance.

Our configuration also shows some robustness to small electron bunch transverse offsets as the bubble generated by the witness bunch wakefield follows the bunch itself. The head of the bunch does not benefit from this effect, and we see some defocusing in this region. This effect is likely to be greater for larger offsets as the bunch oscillates around the axis of the drive bunch wakefield (see right hand plots of figure 6). However, since the proton wakefield creates a quasi linear condition, we still see the head of the beam stabilising after some time. The off-axis case has a larger initial emittance growth (see left hand plots of figure 6), but the growth levels off after the first few metres and stays constant for the remainder of the plasma accelerator section (figure 5).

IV. PARAMETER OPTIMISATION

For accelerator applications in general, and also for Run 2 of the AWAKE experiment, it is desirable to maximise the charge that can be successfully accelerated in the witness bunch. However, a longitudinally constant accelerating field depends on both the position and the charge density of the witness beam [6, 9].

The large number of parameters involved makes the problem difficult to solve in simulations, and difficult to measure in experiments. Presented in figures 7 and 8 is a parameter scan for a matched beam with initial normalised emittance $\epsilon_{N,0} = 2\,\mu$m after propagating through 4 m of plasma. We ran the scan with beam charge from 10 pC to 300 pC and with length σ_z from 40 μm to 100 μm. We see from figure 7 that both the 40 μm and the 60 μm beam has a well defined minimum energy spread with a beam charge ≥ 50 pC and ≈ 100 pC respectively. Lower beam charges tend to underload the field, while higher beam charges tend to overload. It is also clear that long beams with respect to the accelerating flank of the E_z-field, $\approx \lambda_{pe}/4$, will not optimally load the field along its length thus experiencing a larger spread in energy.

A higher charge beam will generate a non-linear wakefield closer to the head of the bunch, which in turns ensures that a smaller portion of the beam experiences the quasi-linear region with emittance growth. As figure 8 illustrates, a higher charge also results in a lower energy gain.

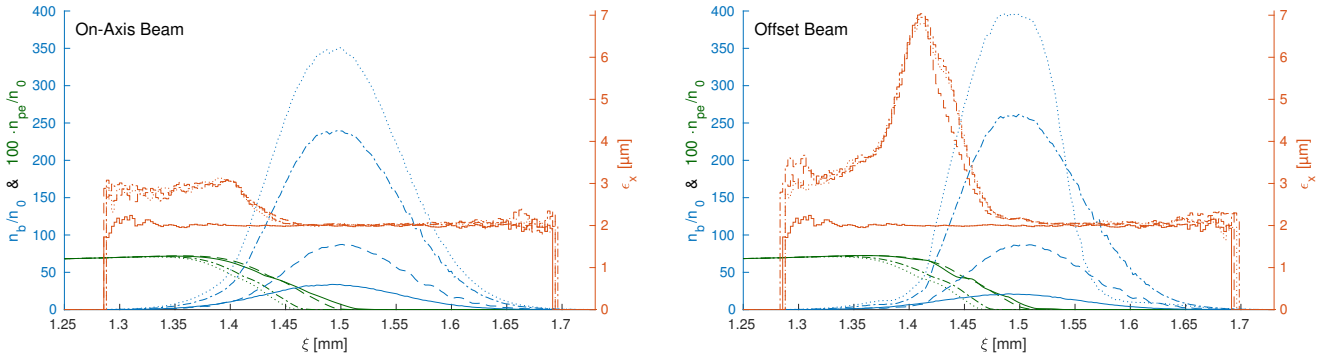

FIG. 5. The red lines show a moving window calculation of transverse normalised emittance for an on-axis beam with respect to the drive beam axis (left) and an offset beam (right) with an offset of one $\sigma_x = 5.24\,\mu$m in the x plane. The moving window for emittance calculation is longitudinal slices of $l = 4 \times \Delta\xi = 18.75\,\mu$m with a $\Delta\xi$ resolution. Only slices with more than 100 macro particles have been included, which accounts for the abrupt edge as well as the noise at either end of the beam due to low statistics. The blue lines show the peak electron beam density profile. For reference, the plasma density profile is included in green, but scaled up by a factor of 100 to be visible. The solid lines are at the plasma entry point, the dashed lines after 4 m of plasma, the dash-dotted after 40 m, and the dotted after 100 m. In order to sustain a stable accelerating field for the witness beam, these simulations were run with an LHC energy drive beam of 7 TeV to avoid de-phasing which causes the structure to break down after about 50 m.

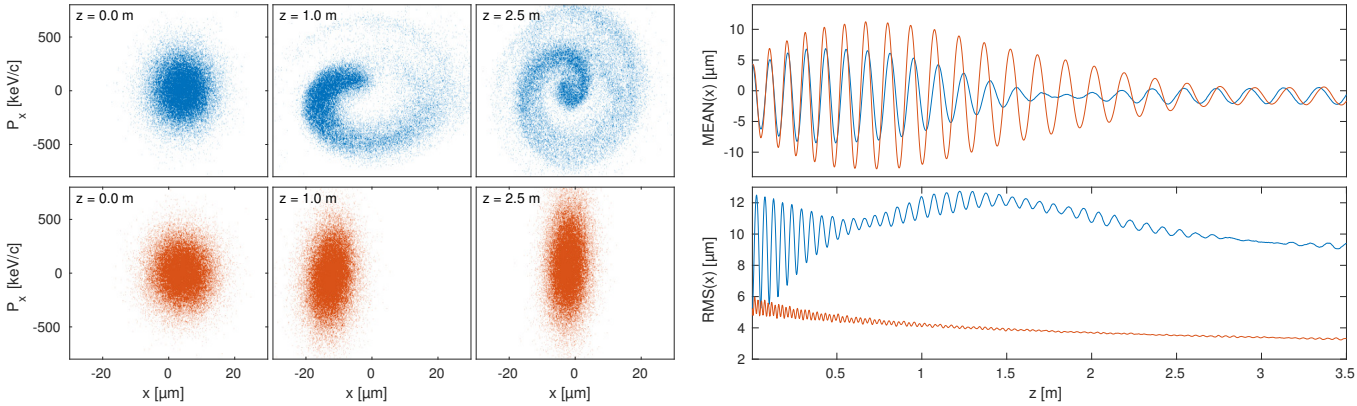

FIG. 6. The left plots show the transverse phase space of the electron beam at different plasma positions. The Right side shows the macro particle mean position (top) and RMS spread (bottom). The blue particles and lines represent particles with position $1.40\,\mu\text{m} < \xi < 1.42\,\mu$m. The red particles and lines represent particles with position $1.55\,\mu\text{m} < \xi < 1.57\,\mu$m.

V. DISCUSSION

VI. CONCLUSION

VII. ACKNOWLEDGEMENTS

The simulations for this study have been run using the open source version of QuickPIC released in early 2017 and owned by UCLA.

These numerical simulations have been made possible through access to the Abel computing cluster in Oslo, Norway. Abel is maintained by UNINETT Sigma2 AS and financed by the Research Council of Norway, the University of Bergen, the University of Oslo, the University of Troms and the Norwegian University of Science and Technology. Project code: nn9303k. Some of the simulations were also run on the student-maintained computing cluster "Smaug" at the University of Oslo, Department of Physics.

The authors would also like to acknowledge the OSIRIS Consortium for providing access to the OSIRIS framework. OSIRIS was used extensively for simulations leading up to the work presented in this paper.

[1] P. Chen, J. M. Dawson, R. W. Huff, and T. Katsouleas, Physical Review Letters **54**, 693 (1985).

[2] J. B. Rosenzweig, D. B. Cline, B. Cole, H. Figueroa,

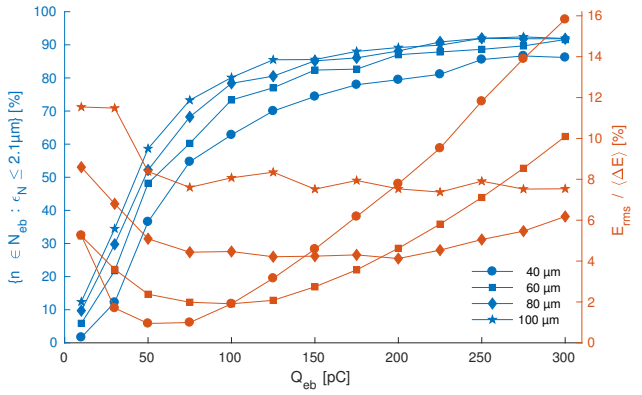

FIG. 7. Ratio of total beam charge with an emittance growth $\Delta\epsilon \leq 5\%$ as a function of initial beam charge (blue), and relative energy spread (red), after 4 m of plasma and with an initial emittance $\epsilon_{N,0} = 2\,\mu$m. These are shown for four different σ_z from 40 μm to 100 μm. The detailed studies presented in beam loading section corrspond to the square marked lines at 100 pC.

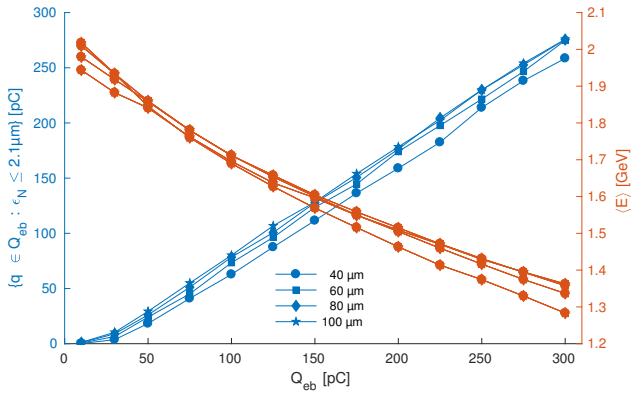

FIG. 8. Total beam charge with an emittance growth $\Delta\epsilon \leq 5\%$ as a function of initial beam charge (blue), and final momentum (red), after 4 m of plasma and with an initial emittance $\epsilon_{N,0} = 2\,\mu$m.

W. Gai, R. Konecny, J. Norem, P. Schoessow, and J. Simpson, Physical Review Letters **61**, 98 (1988).

[3] I. Blumenfeld, C. E. Clayton, F.-J. Decker, M. J. Hogan, C. Huang, R. Ischebeck, R. Iverson, C. Joshi, T. Katsouleas, N. Kirby, W. Lu, K. A. Marsh, W. B. Mori, P. Muggli, E. Oz, R. H. Siemann, D. Walz, and M. Zhou, Nature **445**, 741 (2007).

[4] E. Kallos, T. Katsouleas, W. D. Kimura, K. Kusche, P. Muggli, I. Pavlishin, I. Pogorelsky, D. Stolyarov, and V. Yakimenko, Physical Review Letters **100**, 074802 (2008).

[5] AWAKE Collaboration, R. Assmann, R. Bingham, T. Bohl, C. Bracco, B. Buttenschn, A. Butterworth, A. Caldwell, S. Chattopadhyay, S. Cipiccia, E. Feldbaumer, R. A. Fonseca, B. Goddard, M. Gross, O. Grulke, E. Gschwendtner, J. Holloway, C. Huang, D. Jaroszynski, S. Jolly, P. Kempkes, N. Lopes, K. Lotov, J. Machacek, S. R. Mandry, J. W. McKenzie, M. Meddahi, B. L. Militsyn, N. Moschuering, P. Muggli, Z. Najmudin, T. C. Q. Noakes, P. A. Norreys, E. z, A. Pardons, A. Petrenko, A. Pukhov, K. Rieger, O. Reimann, H. Ruhl, E. Shaposhnikova, L. O. Silva, A. Sosedkin, R. Tarkeshian, R. M. G. N. Trines, T. Tckmantel, J. Vieira, H. Vincke, M. Wing, and G. Xia, Plasma Physics and Controlled Fusion **56**, 084013 (2014).

[6] T. Katsouleas, S. Wilks, P. Chen, J. M. Dawson, and J. J. Su, Particle Accelerators **22**, 81 (1987).

[7] W. Lu, C. Huang, M. Zhou, W. B. Mori, and T. Katsouleas, Physical Review Letters **96**, 165002 (2006).

[8] W. Lu, C. Huang, M. Zhou, M. Tzoufras, F. S. Tsung, W. B. Mori, and T. Katsouleas, Physics of Plasmas (1994-present) **13**, 056709 (2006).

[9] M. Tzoufras, W. Lu, F. S. Tsung, C. Huang, W. B. Mori, T. Katsouleas, J. Vieira, R. A. Fonseca, and L. O. Silva, Physics of Plasmas **16**, 056705 (2009).

[10] P. Muggli, B. Allen, Y. Fang, V. Yakimenko, M. Fedurin, K. Kusche, M. Babzien, C. Swinson, and R. Malone, in *Proceedings of PAC2011* (New York, NY, USA, 2011) pp. 712–714.

[11] A. Caldwell, K. Lotov, A. Pukhov, and F. Simon, Nature Physics **5**, 363 (2009).

[12] N. Kumar, A. Pukhov, and K. Lotov, Physical Review Letters **104**, 255003 (2010).

[13] E. Gschwendtner, E. Adli, L. Amorim, R. Apsimon, R. Assmann, A. M. Bachmann, F. Batsch, J. Bauche, V. K. Berglyd Olsen, M. Bernardini, R. Bingham, B. Biskup, T. Bohl, C. Bracco, P. N. Burrows, G. Burt, B. Buttenschn, A. Butterworth, A. Caldwell, M. Cascella, E. Chevallay, S. Cipiccia, H. Damerau, L. Deacon, P. Dirksen, S. Doebert, U. Dorda, J. Farmer, V. Fedosseev, E. Feldbaumer, R. Fiorito, R. Fonseca, F. Friebel, A. A. Gorn, O. Grulke, J. Hansen, C. Hessler, W. Hofle, J. Holloway, M. Hther, D. Jaroszynski, L. Jensen, S. Jolly, A. Joulaei, M. Kasim, F. Keeble, Y. Li, S. Liu, N. Lopes, K. V. Lotov, S. Mandry, R. Martorelli, M. Martyanov, S. Mazzoni, O. Mete, V. A. Minakov, J. Mitchell, J. Moody, P. Muggli, Z. Najmudin, P. Norreys, E. z, A. Pardons, K. Pepitone, A. Petrenko, G. Plyushchev, A. Pukhov, K. Rieger, H. Ruhl, F. Salveter, N. Savard, J. Schmidt, A. Seryi, E. Shaposhnikova, Z. M. Sheng, P. Sherwood, L. Silva, L. Soby, A. P. Sosedkin, R. I. Spitsyn, R. Trines, P. V. Tuev, M. Turner, V. Verzilov, J. Vieira, H. Vincke, Y. Wei, C. P. Welsch, M. Wing, G. Xia, and H. Zhang, Nuclear Instruments and Methods in Physics Research Section A: Accelerators, Spectrometers, Detectors and Associated Equipment EAAC 2015, **829**, 76 (2016).

[14] V. K. Berglyd Olsen, E. Adli, P. Muggli, L. D. Amorim, and J. Vieira, in *Proceedings of IPAC 2015* (Richmond, VA, USA, 2015) pp. 2551–2554.

[15] E. Adli and AWAKE Collaboration, in *Proceedings of IPAC 2016*, International Particle Accelerator Conference (JACoW, Busan, Korea, 2016) pp. 2557–2560.

[16] R. A. Fonseca, L. O. Silva, F. S. Tsung, V. K. Decyk, W. Lu, C. Ren, W. B. Mori, S. Deng, S. Lee, T. Katsouleas, and J. C. Adam, in *Computational Science ICCS 2002*, Lecture Notes in Computer Science No. 2331, edited by P. M. A. Sloot, A. G. Hoekstra, C. J. K. Tan, and J. J. Dongarra (Springer Berlin Heidelberg, 2002) pp. 342–351.

[17] V. K. Berglyd Olsen, E. Adli, P. Muggli, and J. Vieira, in

Proceedings of NAPAC 2016 (Chicago, IL, USA, 2016).
[18] B. B. Godfrey, Journal of Computational Physics **15**, 504 (1974).
[19] R. Lehe, A. Lifschitz, C. Thaury, V. Malka, and X. Davoine, Physical Review Special Topics - Accelerators and Beams **16**, 021301 (2013).
[20] C. Huang, V. K. Decyk, C. Ren, M. Zhou, W. Lu, W. B. Mori, J. H. Cooley, T. M. Antonsen, and T. Katsouleas, Journal of Computational Physics **217**, 658 (2006).
[21] W. An, V. K. Decyk, W. B. Mori, and T. M. Antonsen, Journal of Computational Physics **250**, 165 (2013).
[22] AWAKE Collaboration and A. Caldwell, *AWAKE Status Report, 2016*, Tech. Rep. CERN-SPSC-2016-033 (CERN, Geneva, 2016).
[23] J. B. Rosenzweig, G. Andonian, M. Ferrario, P. Muggli, O. Williams, V. Yakimenko, and K. Xuan, AIP Conference Proceedings **1299**, 500 (2010).
[24] S. Van der Meer, *Improving the power efficiency of the plasma wakefield accelerator*, Tech. Rep. CERN/PS/85-65 (AA), CLIC Note No. 3 (CERN, Geneva, 1985).